

Summary of the Structure Function Working Group at DIS'99

U. Bassler^a, E. Laenen^b, A. Quadt^c, H. Schellman^d

^aLPHNE, 4 place Jussieu, 75252 Paris Cedex 05, France

^bNIKHEF, Kruislaan 409, 1098 SJ, Amsterdam, The Netherlands

^cCERN, Division EP, 1211 Geneva 23, Switzerland

^dPhysics Department, Northwestern University, Evanston, IL 60210, USA

We summarize the experimental and theoretical results presented in the “Structure Function Working Group - WG1” at DIS'99.

1. INTRODUCTION

The partonic nucleon structure and the underlying dynamics of the quark-gluon interactions, described by QCD, are constrained by Deep Inelastic Scattering experiments and hadron-hadron interactions. In DIS the structure of the proton is probed by a boson exchanged between a lepton and a quark, whereas in hadron-hadron interactions, the cross-section of jet production, the production rates of leptons from Drell-Yan processes or of direct γ , W or Z bosons, are measured. Figure 1 indicates the kinematic regions in x , and Q^2 , of double differential cross-sections in e and ν scattering and of triple differential jet cross-sections measurements in $p - \bar{p}$ collisions¹, presented at the DIS'99 workshop.

The theoretical contributions involved many different aspects of QCD and related theories, and aimed at answering many of the questions raised by more and more precise measurements during the last few years. Presentations were held on parton distribution functions by the major fitting groups and others and different approaches for modeling the proton were discussed. QCD studies involving corrections beyond NLO, and involv-

¹For two jet events, x can be computed in leading order for each of the jets, assuming that the jet is issued from the scattered parton, and $\hat{t} \sim Q^2$ gives the scale of the interaction. Indicated in figure 1 is the measured region in x_{max} , being the highest x value of the two jets in an event and \hat{t} from the CDF triple differential cross-section measurement.

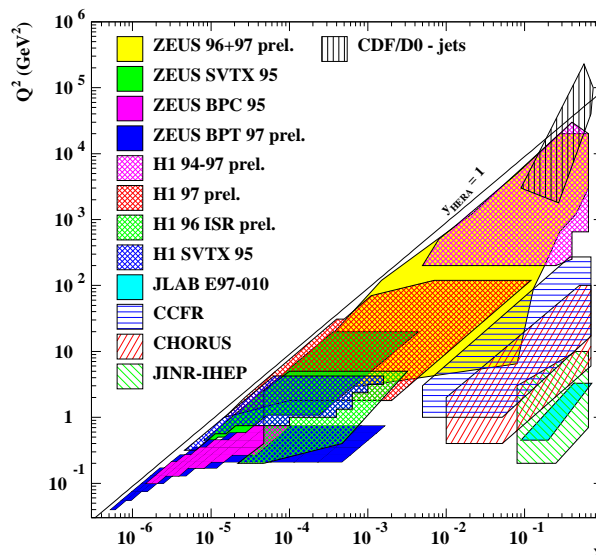


Figure 1. Kinematic regions in $x - Q^2$ for cross-section measurements in Deep Inelastic ep Scattering, ν Scattering and of triple differential jet cross-section measurements in $p\bar{p}$ -collisions.

ing unitarization effects were presented, and new insight was brought to the NLO BFKL-equation.

2. CONSTRAINTS ON PARTON DISTRIBUTION FUNCTIONS

Data from the last two years have had a significant impact on various parton densities, in particular quark ones, motivating the major PDF groups to update their analysis. The GRV'98 [

1] and MRST [2] sets were already introduced at DIS'98. Here, the CTEQ5 [3] set was presented [4]. MRST's Martin and CTEQ's Kuhlmann discussed the impact of these data on their new sets, and compared their results and approaches. The data that spurred these updates (and the densities most affected) are: (i) the more precise ZEUS and H1 data on F_2^p , including F_2^{charm} (sea quarks and gluon), (ii) the NMC and CCFR final muon-nucleon and neutrino-nucleus data, (quarks, u/d), (iii) the E866 pp vs. pd lepton pair production asymmetry ($\bar{u} - \bar{d}$), and the W-charge rapidity asymmetry (u/d), (iv) the final D0 analysis of the inclusive single jet data and the new CDF analysis of this reaction (gluon) and (v) the rather precise direct photon production data from E706 (gluon). An overview of these measurements is given in the following sections.

One clear difference of approach lies in the selection of data for the global analysis that are sensitive to large x gluons. The CTEQ5 set uses the inclusive jet data from the Tevatron to help constrain the large x gluon density, whereas the MRST group employ the prompt photon data of the E706 and WA70 collaborations, together with k_T broadening corrections, to constrain the large x gluon density. Figure 2 shows the comparison of the resulting gluon densities from the CTEQ5 and MRST sets. Clearly there is ample room for better understanding of the large x gluon density.

Perhaps the clearest example of the impact of the new data, in particular those from E866, are the sea quarks \bar{u} and \bar{d} . Where before there was only the NA51 data point, there is now a wide spectrum. The result for the ratio of these densities is shown in figure 3. A similar plot for the CTEQ5 set can be found elsewhere [4] in these proceedings.

The MRST and CTEQ5 heavy flavor densities, in particular charm densities, are distinguished by the adoption of different variable flavor number schemes (VFNS - see section 7 for more on this). We just mention here that the former use the Thorne-Roberts scheme [5], and the latter the ACOT [6] prescription. One should keep in mind that if one wishes to use such densities, the cross section at hand must be computed in the

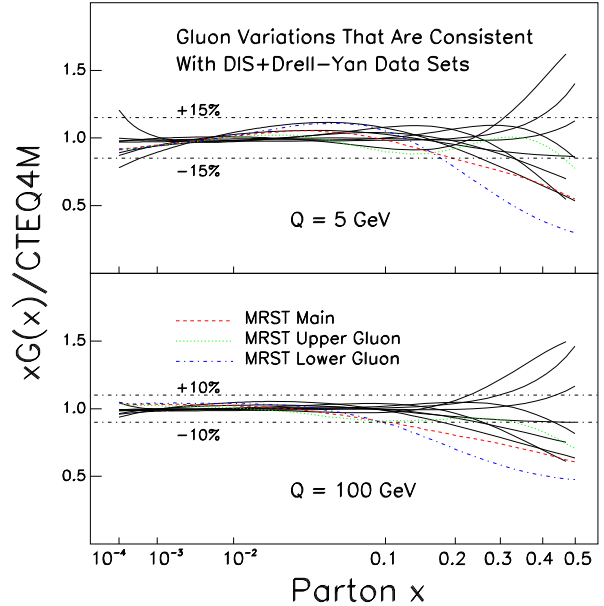


Figure 2. Results of a CTEQ5 gluon density parameter scan, normalized to CTEQ4M (solid lines). Also shown are various MRST densities (dashed lines), see [2] for their definitions.

same scheme used in the construction of these densities.

A important comparison of the two sets [7] consists of the “standard” total Z or W cross sections at hadron colliders. Use of the CTEQ5 set vs. any of the MRST98 for this cross section sets still reveals a worrisome discrepancy of about 5% for Tevatron and LHC energies, only a part of which is due to a small error found in the MRST evolution code, (leading to about 1-1.5% differences in some densities after evolution to $Q^2 = 100 \text{ GeV}^2$ [7]).

An interesting issue was raised after the NMC analysis of the ratio F_2^d/F_2^p , namely whether those data really prefer $d/u \rightarrow 0$, as was always chosen thus far, or rather $d/u \rightarrow 0.2$ [8]. The MRST set essentially fits the data equally well for both kinds of asymptotic behavior, except for the large x data for this ratio [7]. The CTEQ group on the other hand has studied [4] the consequences of incorporating deuterium binding

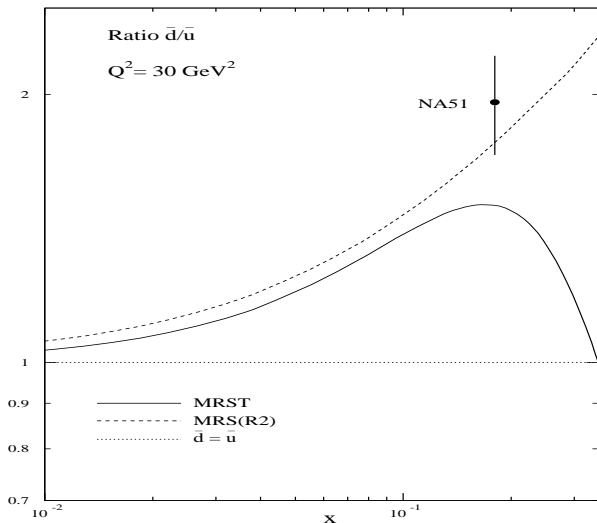


Figure 3. Change in \bar{u}/\bar{d} vs. x with respect to the MRS(R2) result. (From [2].)

effects by refitting their densities, incorporating these effects as derived from the SLAC E139 results, but finds likewise equally good quality fits. Future charged current data at HERA at large x will shed a more definite light on this issue.

Two other NLO global analysis were presented [9, 10], in which mostly deep-inelastic scattering data were used. In the analysis by Botje [9] all experimental (all statistical and 57 sources of systematic) errors were used to actually infer an error correlation matrix on the parameters in his (fixed) PDF parametrization. One outcome of this analysis was that the thus established errors on the parton densities leave one unable to confirm or rule out the just-mentioned suggestion [8] for the d/u behavior at large x , see fig. (4), a conclusion reached more indirectly by the MRST and CTEQ groups. Furthermore, large Q^2 charged current ZEUS scattering data for $d\sigma/dQ^2$ were found to agree very well with the calculation and error of this quantity using these PDF's.

In Zomer's analysis [10], which includes, among other, a considerable amount of neutrino scattering data (including some revived older CDHSW iron-target data) the main goal is to examine differences between the s and \bar{s} densities (while keeping the net strangeness number

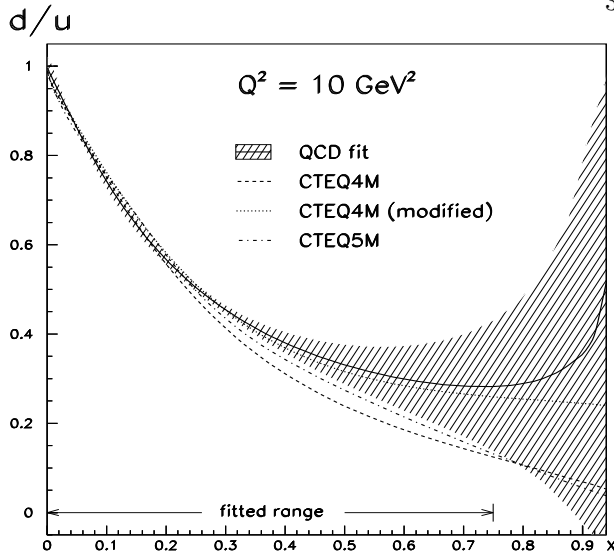


Figure 4. The ratio $(d + \bar{d})/(u + \bar{u})$ from the QCD fit compared to CTEQ densities, see [9]. The hatched band shows the error on the QCD fit.

zero). After carefully taking into account nuclear corrections, and eliminating possible higher twist contributions by cuts on Q^2 and W^2 , the $xs(x)$ distribution was found to be significantly harder than $x\bar{s}(x)$ at x values larger than about 0.5.

3. STRUCTURE FUNCTIONS MEASUREMENTS

Besides the published HERA measurements used in the fitting programs of CTEQ, GRV and MRS, preliminary results of structure function measurements with significantly increased precision were presented from the high statistic 96 and 97 data by the H1 and ZEUS collaborations.

The presented measurements of ν -Scattering are in the high x , low Q^2 region, accessible with ν beam energies between 6 GeV and 360 GeV on massive targets as Iron (CCFR), Lead (CHORUS) or Aluminum (IHEP-JINR).

3.1. ep SCATTERING

After five years of operation of HERA, the F_2 structure function measurements span over 5 orders of magnitude in x and Q^2 [11, 12]. Figure 5 shows F_2 as function of Q^2 for various values of

x . After precise measurements from fixed target experiments at low Q^2 , high x , HERA explored in the first years of operation especially the low x region, where the rise of the structure function with decreasing x was established. Additional de-

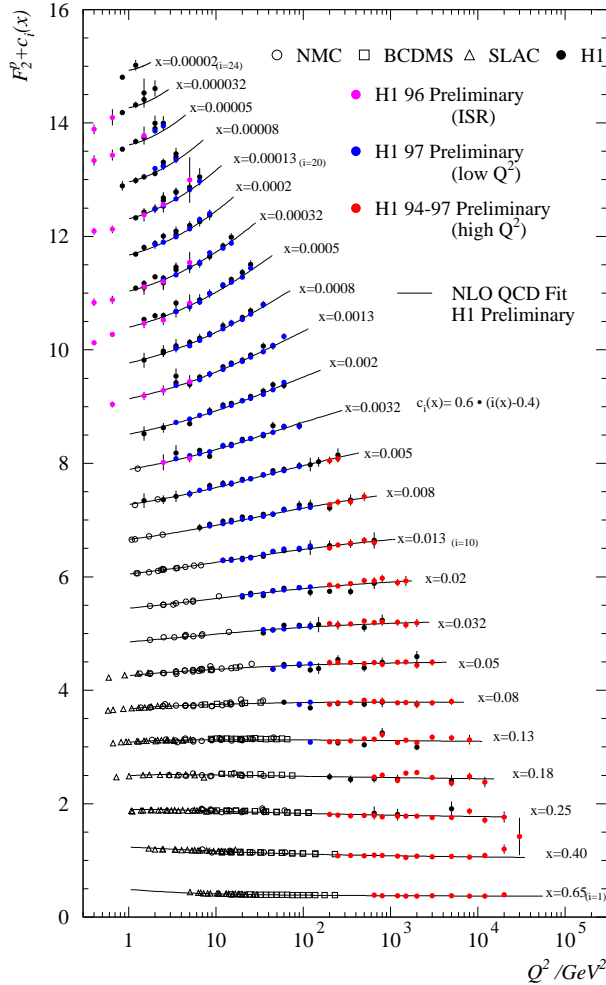


Figure 5. F_2 as function of Q^2 for fixed values of x from H1, NMC, BCDMS, E665 and SLAC. The results from the ZEUS experiment are compatible with the shown H1 measurement.

tector devices and special runs gave access to the the very low Q^2 region and clarified the transition towards photoproduction, which will be discussed in more detail in section 9. Increased luminosity

allowed for measurements in the high Q^2 , high x domain.

Compared to the 1994 measurements [13], the integrated luminosity increased by a factor ~ 10 , such that the measurements are dominated by the systematic errors in the high precision medium Q^2 range. In this kinematic region, the increased statistics allowed for a better understanding of the systematic effects, leading to an overall error on the structure function measurement of 3–4%. The H1 collaboration performed a detector upgrade in the backward region, replacing in 1995 the Backward Electromagnetic Calorimeter by a SpaCal and the former Backward Proportional Chamber by a Drift Chamber and adding in 1997 a Backward Silicon Tracker, which allowed to extend the kinematic reach towards higher y and lower Q^2 .

The scaling of the structure function, as expected if the proton was made from pointlike, non-interacting partons, can be observed in the valence region at $x \sim 0.3$. At low x however, the quark-gluon interactions must be considered, and from the observed scaling violation the gluon density, being responsible for the rise of F_2 at low x , can be extracted, taking into account theoretical and experimental systematic errors, with an actual precision of $\sim 10\%$. NLO QCD-fits performed by the collaborations, are in good agreement with the data over the whole kinematic domain, even at Q^2 values as low as 1 GeV^2 . Studies on the evolution of the gluon density by the ZEUS collaboration showed a flat behaviour as function of x of the gluon at low scale, $Q^2 = 1 \text{ GeV}^2$, whereas the singlet quark densities in this kinematic region is still rising.

Assuming the validity of QCD, the longitudinal structure function F_L can be extracted [14] from the cross-section measurement at high y , either by subtracting from the measured cross-section the contribution of F_2 [15], determined from a NLO-QCD fit in the low y region, or from the derivative of the reduced cross-section $d\tilde{\sigma}/dy$. From Figure 6, showing F_L as the result of these procedures as function of Q^2 for two different y -values, $F_L = F_2$ can be excluded. At high y , the extracted F_L values are slightly above the expectation from the QCD-fit.

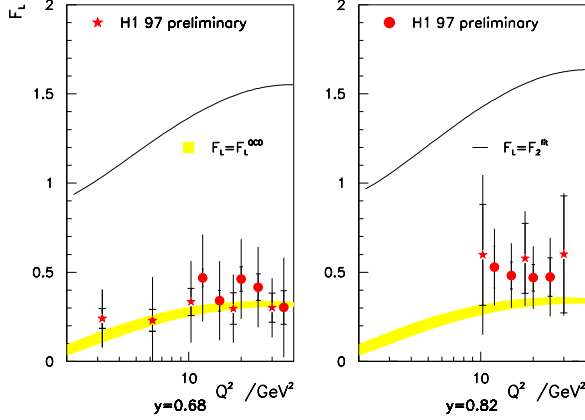


Figure 6. F_L as function of Q^2 for $y = 0.68$ and $y = 0.8$ extracted from the cross-section measurements by H1.

3.2. NEUTRINO SCATTERING

The CCFR experiment at Fermilab uses mixed ν_μ , $\bar{\nu}_\mu$ neutrino beams, produced from the Tevatron proton beam, with energies between 30 – 360 GeV. With 2000k events accumulated in their final sample, an increased precision in cross-sections measurements compared to previous measurement of CDHSW is achieved [16]. Figure 7 shows the $1/Ed^2\sigma/dxdy$ cross-section from CCFR for ν and $\bar{\nu}$, at low x with $\langle E_\nu \rangle = 150$ GeV. Together with the measurements at $E_\nu = 85$ GeV, they were presented for the first time, as previously only the extracted structure function were available [17] and will allow for detailed QCD analysis. Overall a good agreement with CDHSW [18] is observed. Within the framework of QCD, F_2 , $\Delta x F_3$ and R can be extracted. $\Delta x F_3 = 4x(c + s)$, when extracted with $m_c \neq 0$ is described by calculations of the charm contribution using the *VFS* and *MFS*.

The Chorus experiment at CERN [19], took data for the search of $\nu_\mu \rightarrow \nu_\tau$ oscillations until 1997. During the 1998 running, the detector could be used for cross-section measurements [20], and 1600k ν and 200k $\bar{\nu}$ interactions with $10 \text{ GeV} < E_\nu < 240 \text{ GeV}$ are currently analyzed.

At even lower ν -beam-energies $6 \text{ GeV} < E_\nu <$

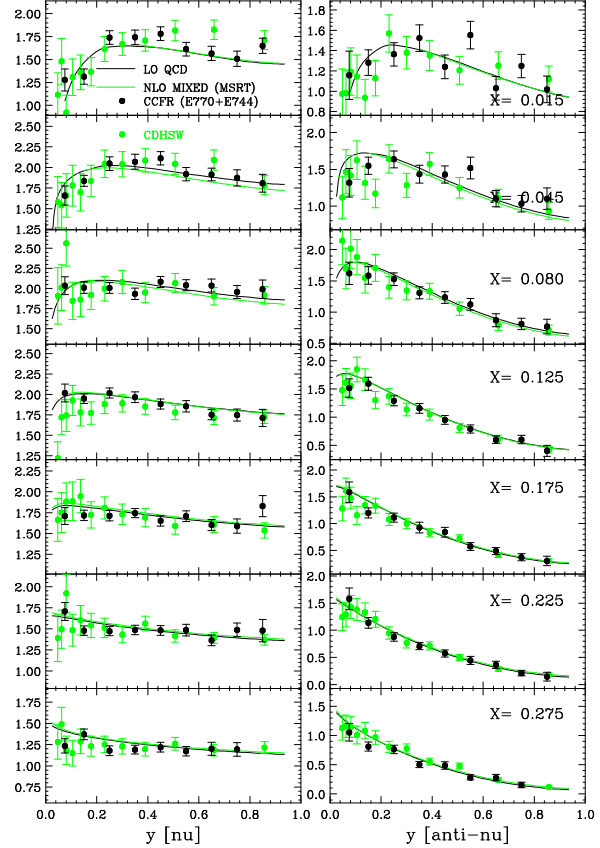


Figure 7. Cross-section (in 10^{-38} cm^2) of deep inelastic ν and $\bar{\nu}$ scattering at $\langle E_\nu \rangle = 150$ GeV as function of y at different values of x from the CCFR experiment compared to the CDHSW measurement.

28 GeV, the IHEP-JINR experiment measures F_2 and $x F_3$ [21]. Within the low statistics accumulated ($6k \nu$ and $0.7k \bar{\nu}$), the extracted value of $\alpha_S = 0.123^{+0.010}_{-0.013}$ agrees with the CCFR measurement. Higher statistics in this low Q^2 region would be very useful for further testing of the GLS-sum rule.

4. \bar{d}/\bar{u} ASYMMETRY

The observation by NMC of the violation of the Gottfried Sum Rule [22], predicting the integral

over x of the difference between F_2^p and F_2^n to be $1/3$, resulted in an interpretation of the existence of a global flavour asymmetry, under the assumption that isospin symmetry is verified.

New measurements from the HERMES [23] collaboration on the asymmetry of the light flavour sea-quarks are comparing charged pion yields in semi-inclusive DIS on hydrogen and deuterium targets and are confirming the NMC result. After integration at $Q_0^2 = 2.5 \text{ GeV}^2$, the two results are:

$$\text{HERMES : } \int_0^1 (\bar{d}(x) - \bar{u}(x)) dx = 0.16 \pm 0.03$$

$$\text{NMC : } \int_0^1 (\bar{d}(x) - \bar{u}(x)) dx = 0.147 \pm 0.039$$

The NuSea-experiment (E866) [24], measures the ratio of muon pair yields from Drell-Yan production of proton-proton or proton-deuteron interactions. From this ratio, the \bar{d}/\bar{u} ratio is determined. Using $\bar{d}+\bar{u}$ from the CTEQ4M parametrisation, $\bar{d}-\bar{u}$ is extracted. At $Q_0^2 = 50 \text{ GeV}$ the integration yields to :

$$\text{NuSea : } \int_0^1 (\bar{d}(x) - \bar{u}(x)) dx = 0.115 \pm 0.008$$

A comparison of the $\bar{d}-\bar{u}$ measurement from HERMES and NuSea is shown in figure 8. The $\bar{d}-\bar{u}$ difference is increasing towards low x , thus an important contribution to the integrated values is coming from the unmeasured region at low x . Although the two measurements are at different Q^2 values, no difference can be observed within the present errors.

Szczurek [25] discussed the E866 [24] and HERMES [23] data that impact the sea quark densities, in the context of pion cloud models. In such models one expands the proton wave function into hadronic Fock states, the leading ones containing one pion

$$|p\rangle = c_0|p\rangle + c_1|n\pi^+\rangle + c_2|p\pi^0\rangle + \dots \quad (1)$$

The idea is that the components involving a single pion (being the lightest meson these fluctuations have the longest lifetime) are chiefly responsible for the sea quarks. Originally these models were conceived to help understand the violation of the Gottfried Sum Rule. As long as only one Drell-Yan data point was available to help constrain the

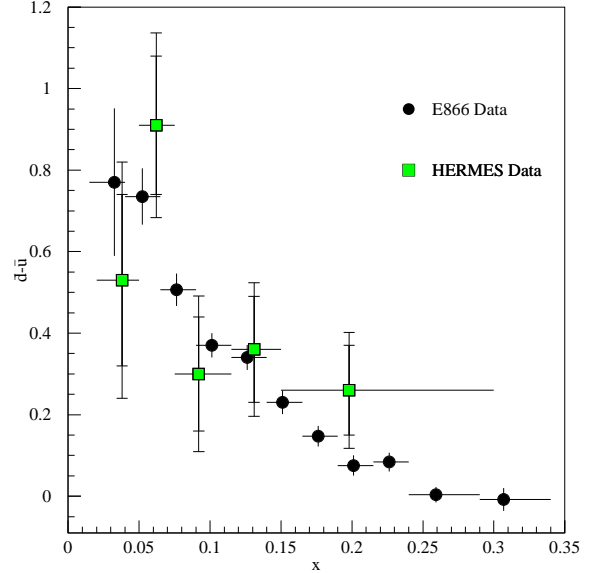


Figure 8. $\bar{d}-\bar{u}$ from NuSea (E866) and HERMES as function of x .

model, a simple model sufficed. The recent measurement of the x -shape [24], and in particular the diminishing of $\bar{d}-\bar{u}$ at larger x , led to a reconsideration [25] of this model. In this analysis, the model enlisted, via Regge factorization, and using unitarity arguments, leading pion, nucleon and Δ data to help constrain it. Overall consistency, including the vanishing of $\bar{d}-\bar{u}$ at larger x , was found, and the Fock states listed on the right in Eq. (1) were indeed seen to be the ones that are mainly responsible for the $\bar{d}-\bar{u}$ asymmetry. In addition, caveats were placed next to some of the factors in the LO formula used to relate the $\bar{d}-\bar{u}$ asymmetry to the data [25].

5. QUARK-DISTRIBUTIONS AT HIGH x

Besides the measurement of the structure functions at high x in DIS, the production of W or Z bosons from $q-\bar{q}$ annihilation in high energetic $p-\bar{p}$ collision provides independent information on the high x parton densities [26].

The CDF collaboration extended the measure-

ment of Z -production [27] up to rapidities of 2.5, corresponding to x values up to 0.61. The production rate over the entire rapidity range is well described by the NLO-QCD calculation [28] or including gluon resummation (VBP) [29] on LO-PDF's.

Compared to the Z -production, the W production [30] is sensitive to different quark flavours, as $W^+(W^-)$ is primarily produced from $u - \bar{d}(d - \bar{u})$ annihilation from the $p - \bar{p}$ interaction. The charge asymmetry in the W production as function of y is therefore related to the difference in the momentum distribution of the u and d quark. Although the W rapidity is not directly measurable, the charge asymmetry in the production of the subsequent leptons is still sensitive to the parton distribution functions (figure 9), and constrain the u/d ratio in an x range of 0.004 to 0.3 at $Q^2 \sim M_W^2$.

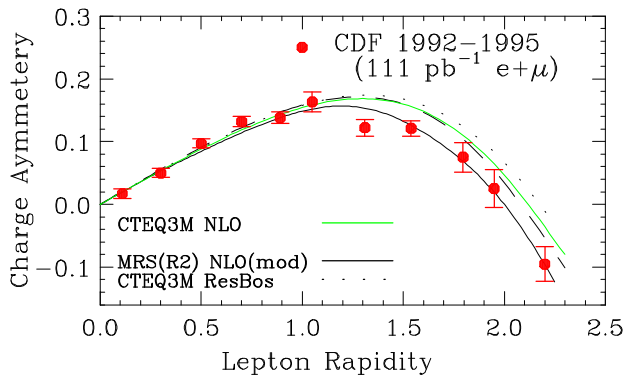


Figure 9. Charge asymmetry for W production as function of the rapidity of subsequent lepton measured by CDF.

The direct comparison of u/d distributions obtained from the ratio of F_2^n/F_2^p from NMC data taking into account effects of nuclear binding of the deuteron, showed disagreement at high x with the W charge asymmetry. As the u valence distribution is strongly constrained by F_2^p data, applying deuteron corrections lead to a modification in the d distribution at high x and the mod-

ified parton densities give better agreement with various other data sets [8]. The applied deuteron corrections, obtained from a reanalysis of SLAC data [8] are based on a model of Frankfurt and Strikman [31], and smaller than the theoretical predictions from Melnitchouk and Thomas [32].

Supplementary constraints on the quark densities at high x , in particular on the d -quark, are expected from the HERA cross-section measurements at high x and high Q^2 , for both charged and neutral currents.

During the 1994-1997 running, HERA was producing e^+p interaction, therefore the charged current cross-section, based on a W^+ -boson exchange, is dominated by the d -valence contribution in the high x region (figure 10) [33, 34, 35]. With the presently integrated luminosity, these measurements are still dominated by the limited statistics.

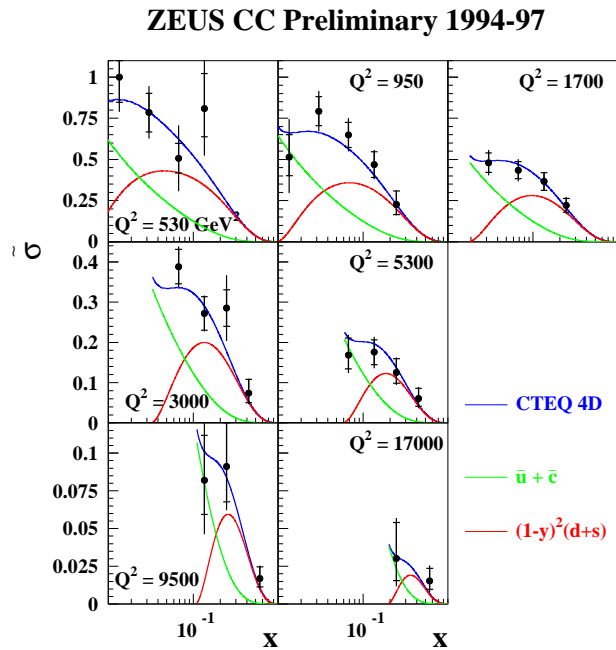


Figure 10. Reduced charged current cross-section as function of x in bins of Q^2 from ZEUS compared to CTEQ4D. Indicated are the $\bar{u} + \bar{c}$ and the $d + s$ contributions to the cross-section. H1 presented a similar measurement.

The neutral current-cross section in e^+p scattering is expected to have a flat behaviour in x at low Q^2 , where only γ exchange occurs, and to decrease at high Q^2 , due to the negative $\gamma - Z$ interference, which can be observed in figure 11, except at $x = 0.45$, where the excess of events at high Q^2 observed by H1 and ZEUS in the 94 – 96 data [36], are located in the H1 case. Although the errors in this kinematic region are large, due mainly to the limited statistics, the inclusion of these data in NLO QCD-fits will improve the precision on PDF's.

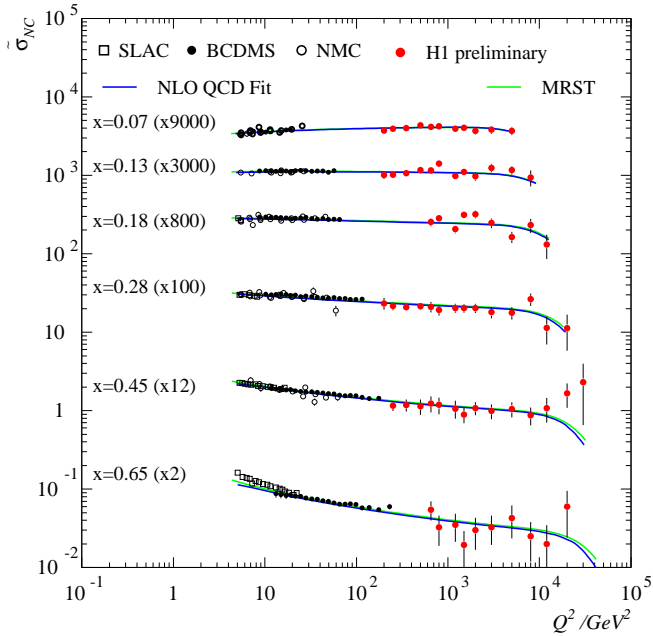


Figure 11. *Reduced neutral current cross-section as function of Q^2 for different values of x in the high x region from H1 data.*

At low Q^2 , the electroproduction of resonances at very high x is a non-perturbative phenomena, although quark-hadron duality implies the average of the resonance strength to be similar than in DIS. The results of the E97-010 experiment at JLAB [37], measuring F_2 proton and F_2 deuteron in the resonance region (figure 12), show indeed the structure functions oscillation

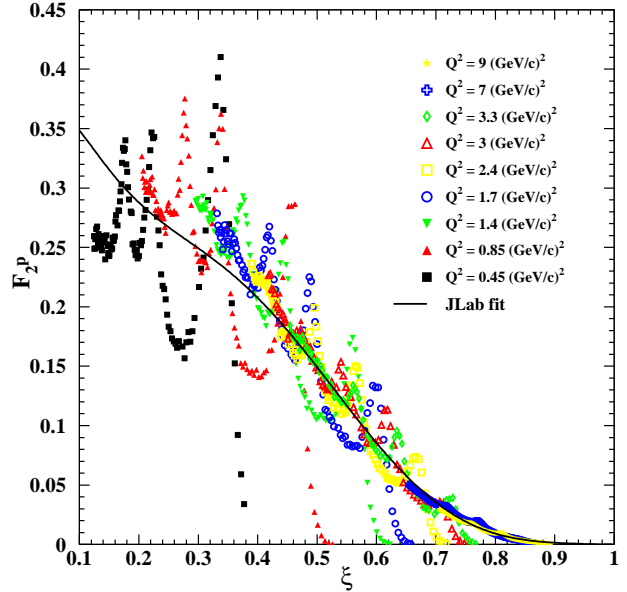


Figure 12. F_2^p as function of x for various Q^2 values in the resonance region from the E97-010 experiment.

around an average curve. In this figure F_2 is plotted as a function of the Nachtmann variables $\xi = 2x/(1 + \sqrt{1 + 4M^2x^2/Q^2})$, in order to take target mass corrections into account.

6. THE GLUON AT HIGH x

Even though the quark-densities at high x will be further constrained by HERA data, the gluon density in DIS can be mostly constrained up to $x \sim 0.1$ from jet production. Constraints on the gluon density at high x are obtained from jet-cross section measurements at the Tevatron and prompt photon production.

Earlier measurements of the inclusive jet cross-section of CDF, showed an excess of the jet-rate at high E_T , which could be interpreted as indication of quark-substructure [38, 39]. A refined analysis and similar measurements from DØ [40, 41], which give a lower cross-section but are still compatible with CDF, showed that also an enhanced gluon density at high x could explain this result. Using the complete statistics of the Tevatron Run

I, allowed for measurements of the triple differential dijet cross-section $d\sigma/dE_T d\eta_1 d\eta_2$.

The CDF cross-sections [42], correspond to events, where a central jet determines the E_T of the event and a second jet is detected in any of four η bins (figure 13), while the DØ measurement

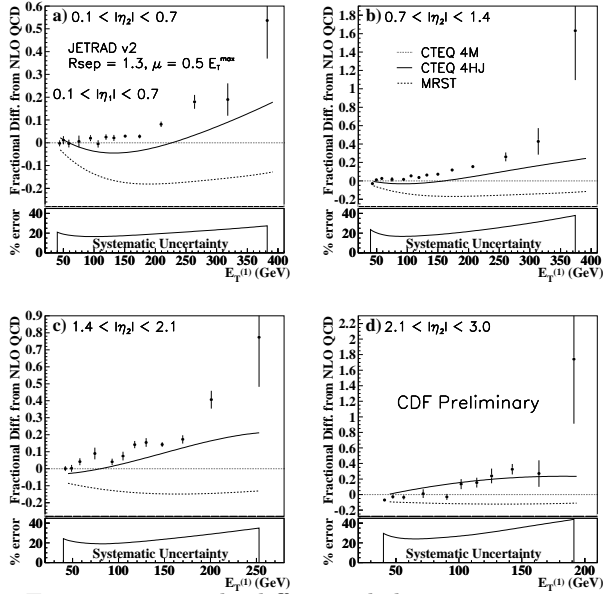


Figure 13. Triple differential dijet cross-section from CDF compared to JETRAD calculation with various PDFs.

[43] requires the both jets to be in the same bin of η , but differentiates between same side and opposite side jets (figure 14). Both measurements are compared to different PDFs using JETRAD calculations.

Direct γ are mainly produced by Compton Scattering as $gq \rightarrow \gamma q$, and gives therefore a constraint on the gluon density at high x . Cross-section measurements for direct γ production are available from the E706 fixed target experiment [44, 45], where 515 GeV π^- or 530 GeV or 800 GeV p beams are scattered on Be , Cu or H targets and from CDF in $p\bar{p}$ collisions. NLO-calculations show deviations from the expected cross-sections, as shown in figure 15 for the E706 measurement.

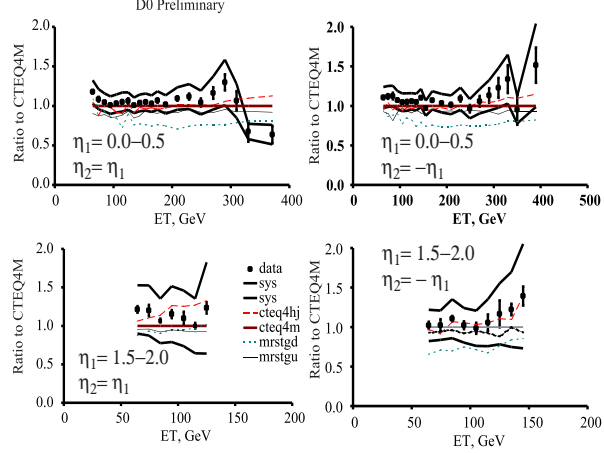


Figure 14. Triple differential dijet cross-section from the DØ experiment compared to JETRAD calculation with various PDFs.

These deviations are mainly due to initial state soft-gluon radiation, which are producing an ini-

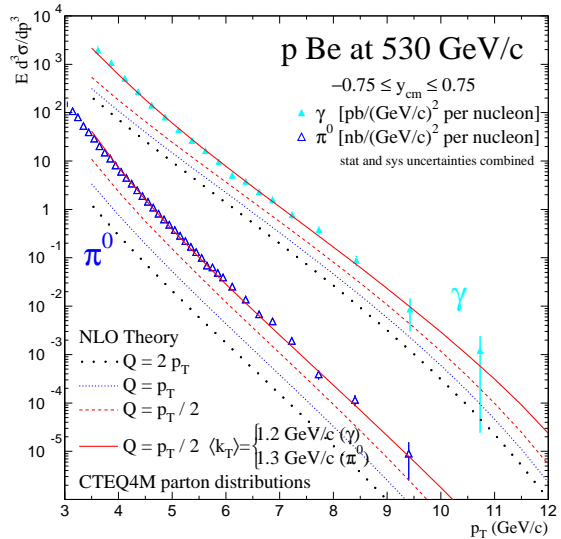


Figure 15. Invariant cross sections for direct- γ and π^0 production in the E706 experiment compared to NLO order calculation with different scales and with additional K_T enhancement.

tial k_T for the interacting partons. Figure 16 shows Q_T , the sum of p_T of the outgoing photons in di- γ events, which is clearly not described by NLO [46], which does not take soft gluon radiation into account, as done in the resummed calculation (RESBOS) [29]. This effect can be approximated by introducing Gaussian k_T smearing in LO calculations as shown in the PYTHIA distribution. A good description of the E706 cross-sections is obtained with $\langle k_T \rangle$ of 1.1 GeV, whereas for the CDF data [47] at higher center of mass energy, deviations from the NLO-cross section are only seen in the low p_T region ($p_T < 50$ GeV) and require a $\langle k_T \rangle$ of 3.5 GeV.

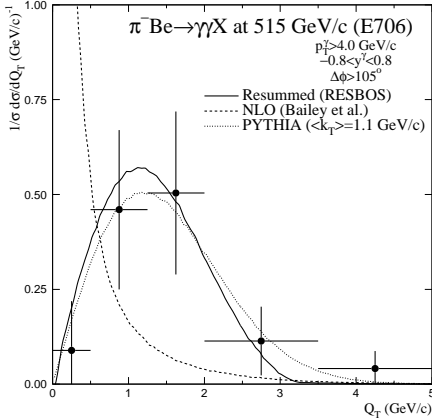


Figure 16. Sum of p_T of outgoing direct- γ pairs seen in the E706 experiment, compared to NLO expectations, resummed calculations. Effects of soft gluon radiation emulated by k_T smearing in PYTHIA.

6.1. F_2^c CHARM

Charm production in DIS is obtained from Photon-Gluon Fusion, and therefore directly coupled to the gluon density. The contribution of charm to F_2 has been measured at HERA from D^* production or tagging of semileptonic decays [48, 49, 50]. In order to extract F_2^c , the “seen” contribution, which corresponds to 25% – 70%, has to be extrapolated to the full phase space. Be-

sides uncertainties from the fragmentation model of the c-quark to the D^* meson have to be taken into account: comparison by ZEUS of the $d\sigma/d\eta$ may indicate a better description using fragmentation models as JETSET or HERWIG, than the Peterson Fragmentation which was developed for e^+e^- interactions and does not take into account colour strings between the proton remnant and the struck quark.

As the charm production is related to the gluon density, F_2^c shows scaling violation behaviour (figure 17), which is described by NLO-OCD [51],

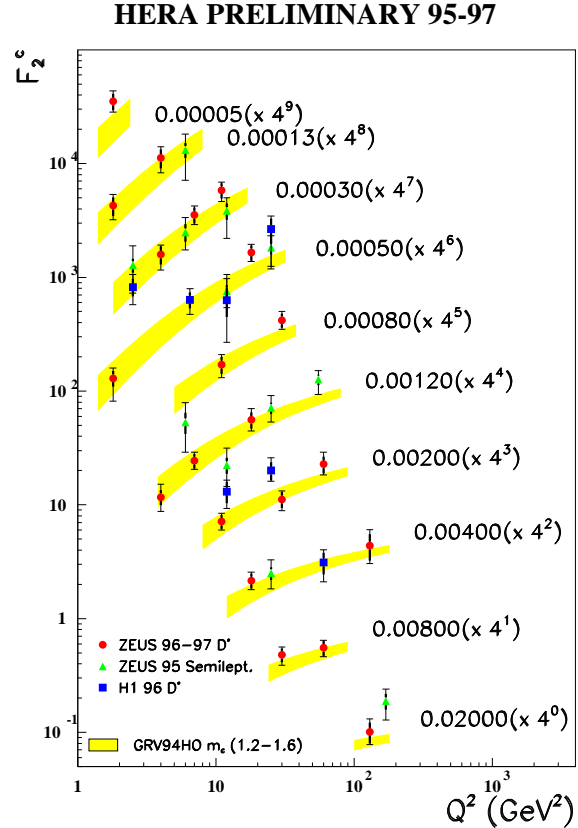


Figure 17. F_2^c from the H1 and ZEUS collaborations as function of Q^2 for various x values.

and stronger than for the inclusive F_2 . The charm contribution to the inclusive F_2 accounts for $\sim 25\%$ at low x . With the increased statistics

of the 95 – 97 data sample the rise in F_2^c at low- x can now be seen for the first time in a single experiment.

7. HEAVY FLAVORS

The issue of what description to use for heavy flavor production in any collision with initial hadrons, such as deep-inelastic scattering, is a subtle one. One must decide whether one wants to employ a fixed number of light flavors in the evolution of the parton densities and α_s and treat the heavy flavor as an external quantum field: the “fixed flavor-number scheme” (FFNS); or whether one wishes to change the number of dynamical flavors depending on the scale present in the parton subprocess: the “variable flavor-number scheme” (VFNS). An overview of present approaches, and a review of the main concepts was presented by Smith [52].

Although the FFNS is more straightforward in use, and has been the scheme of choice for almost all available NLO calculations of heavy flavor production, it can suffer from large perturbative corrections proportional to $\alpha_s \ln(Q^2/m^2)$ when the hard scale Q of the reaction is significantly larger than the heavy quark mass m . The VFNS then provides a mechanism to resum such logarithms, without relinquishing control over the region $Q \simeq m$.

The VFNS exists in various implementations [6, 5, 53]. These mainly differ in the treatment of the transition region. The proper transitions are encoded in matching conditions for α_s [54] and the PDF’s [53], which are now both known to NNLO. A couple of lessons learned in developing VFNS concepts were pointed out [52]. The first is that any parton density should really be referred to with a label indicating the number of flavors. Thus, the n_f -flavor gluon density is related by a (in general discontinuous) matching condition to the $n_f + 1$ -flavor gluon density at the matching scale μ_0 , typically the mass of the extra heavy flavor.

Above the matching scale μ_0 , the heavy flavor enters with its own density $c(x, \mu)$ (taking the example of charm). The second lesson is that the NNLO matching conditions may in fact ren-

der $c(x, \mu_0)$ negative [52] which will noticeably change the size of the $n_f + 1$ -flavor gluon density, and charm density at scales above the matching scale, compared to their sizes resulting from the NLO matching condition $c(x, \mu_0) = 0$.

Third, the distinction between F_2^{charm} and F_2^{light} becomes somewhat arbitrary from $\mathcal{O}(\alpha_s^2)$ onwards. E.g. in initial light quark channels, cubic logarithmic contributions from Compton-like processes where the gluon splits into a $c\bar{c}$ pair, would be canceled by those from charm loop contributions to gluon radiation processes, were it not that one would naively assign the former to F_2^{charm} and the latter to F_2^{light} . A possible resolution of this issue, involving an acceptance cut on the charm pair invariant mass, was also discussed [52].

8. OTHER NLO-AND-BEYOND STUDIES

There were a number of presentations that involved studies of tools and properties of perturbative QCD quantities occurring at NLO, and beyond.

The power of Mellin transforms $\tilde{f}(N) = \int_0^1 dx x^{N-1} f(x)$ and harmonic sums as tools in NNLO calculations was shown by Blümlein [55]. Mellin transforms turn convolutions into simple products. Harmonic sums are defined by

$$S_{k_1, \dots, k_m}(N) = \sum_{i_1}^N \left(\frac{(\text{sign}(k_1))^{i_1}}{i_1^{|k_1|}} \right) \cdots \sum_{i_m}^{i_{m-1}} \left(\frac{(\text{sign}(k_m))^{i_m}}{i_m^{|k_m|}} \right). \quad (2)$$

Using such sums, a dictionary [55] can be established for a complete basis of functions of x occurring in massless QED and QCD, so that translation from Mellin space to x space is very straightforward. For NNLO, one only needs $|k_1| + \dots + |k_m| \leq 4$. There are many simplifying relations between harmonic sums, reducing the number of sums needed for the dictionary. E.g. the relation $S_{n,m} + S_{m,n} = S_m S_n + S_{m+n}$, $m, n > 0$ expresses two-fold sums into single ones.

The spacelike DIS process $e^-(k) + P(p) \rightarrow$

$e^-(k-q) + X$ and the timelike annihilation process $(e^+e^-)(q) \rightarrow P(p) + X$, enjoy, under certain conditions, a crossing property known as the Drell-Levy-Yan (DLY) relation, for the corresponding hadronic tensors $W_{\mu\nu}^T = W_{\mu\nu}^S(-p, q)$. Both tensors can be expressed in structure functions F_i , $i = 1(2), L$. In this language, the time-like (T) structure functions can be viewed, if DLY holds, as the analytic continuation (Ac) beyond $x = 1$ of the spacelike (S) ones:

$$F_i^T(x_E, Q^2) = x_B \text{Ac} \left(F_i^S \left(\frac{1}{x_B}, Q^2 \right) \right),$$

$$x_E = \frac{2p \cdot q}{Q^2}, \quad x_B = \frac{Q^2}{2p \cdot q}. \quad (3)$$

QCD factorization tells us that each structure function can be decomposed into sums over partons l of coefficient functions C_l^i convoluted with PDF's f_l , where the evolution of the latter is controlled by a kernel consisting of (a matrix of) splitting functions. The validity of the DLY relation was examined by Ravindran [56] for coefficient functions, splitting functions, and physical observables, through NLO. It was shown that the DLY relations for both splitting functions and coefficient functions are violated, but that these violations can be seen as factorization scheme variations. Hence for scheme invariants, such as structure functions, the DLY relation holds.

An extensive NLO-and-beyond analysis [57] of the CCFR xF_3 data examined the effects of including ever higher orders on $\alpha_s(M_Z)$ and on a possible twist 4 component of the data. The Mellin-moments $M_N(Q^2)$ of this structure function can, after solving the DGLAP equation from scale Q_0 up, be written as

$$\frac{M_N(Q^2)}{M_N(Q_0^2)} = \left(\frac{\alpha_s(Q^2)}{\alpha_s(Q_0^2)} \right)^{\frac{\gamma^{(0)}}{2\beta_0}} \times \frac{\text{Ad}(N, \alpha_s(Q^2)) C_N(Q^2)}{\text{Ad}(N, \alpha_s(Q_0^2)) C_N(Q_0^2)} \quad (4)$$

with $\gamma^{(i)}$, β_i the N^i LO anomalous dimension and beta function. The coefficient function C_N and the perturbative expansion of the evolved parton distribution function Ad are expanded to LO, NLO, NNLO, and N³LO, where unknown quan-

tities at NNLO and N³LO, such as $\gamma^{(2)}, \gamma^{(3)}$, are estimated with Padé approximations.

A translation to x -space can be established by expanding $xF_3(x, Q^2)$ in a series of integer moments as in (4), with coefficients expressed in Jacobi polynomials. In addition, a twist-4 term $h(x)/Q^2$ is allowed. The data are then fitted for $\Lambda_{\overline{\text{MS}}}^4$ and the size and shape of the twist-4 term. Besides increasing the perturbation order, the effects of varying Q_0 , the type of Padé approximant, among others, were investigated. The main findings are, first, a NLO and NNLO $\alpha_s(M_Z)$ value around 0.120, with, when also considering the LO result, a clearly convergent behavior and second, a decrease in size of the inferred twist 4 contribution per higher order included at leading twist, and an increase of $h(x)$ near $x = 1$.

A very different method of obtaining well-defined NLO and NNLO estimates of $\alpha_s(M_Z)$, involving scheme-invariant evolution of structure functions, was presented by Vogt [58]. The evolution in Q^2 of the inclusive structure functions F_2^S , F_2^{NS} and F_L is conventionally understood as being implicitly governed by the DGLAP evolution in the factorization scale μ of the parton distribution functions entering the factorized description of these structure functions

$$F_i(x, Q^2) = \sum_l \left[C_l^i \left(\frac{Q^2}{\mu^2} \right) \otimes f_l(\mu^2) \right] (x, Q^2) \quad (5)$$

where \otimes indicates the convolution symbol. Because this evolution is only due to QCD interactions, its precise determination is a well-used method for determining α_s . The coefficient functions C_l^i and the universal anomalous dimensions $\gamma_{ff'}$ that determine the DGLAP evolution are however scheme dependent, so that one must be careful to ensure that scheme dependence cancels between the C 's and the f 's when calculated to a given order in perturbation theory. A very significant source of theoretical uncertainty in measuring α_s are the f 's: for determining the evolution of the above-mentioned three structure functions, knowledge of many parton distribution functions is required in eq. (5). Automatic incorporation of scheme independence and elimination of the PDF uncertainty is achieved via scheme-invariant evo-

lution (the concepts of which were also discussed by Ravindran [56])

$$\frac{d}{d \ln Q^2} \begin{pmatrix} F_2 \\ F'_L \end{pmatrix} = \begin{pmatrix} P_{22} & P_{2L} \\ P_{L2} & P_{LL} \end{pmatrix} \begin{pmatrix} F_2 \\ F'_L \end{pmatrix} \quad (6)$$

The “physical” anomalous dimensions P_{AB} are combinations of the DGLAP ones and the coefficients, and hence process dependent. However, they are a computable perturbative series in α_s . The NLO $\alpha_s(M_Z)$ determined [58] in this way is

$$\alpha_s(M_Z) = 0.114 \pm 0.002(\text{exp}) \pm \begin{pmatrix} 0.006 \\ 0.004 \end{pmatrix} (\text{th}) \quad (7)$$

The extension of this to NNLO was also presented [58], for the non-singlet structure function F_2^{NS} , using all available NNLO information (see [58] for details), with the uncertainty due the unknown part of the NNLO anomalous dimension quantified, see fig. (18) At large x the NNLO curve is

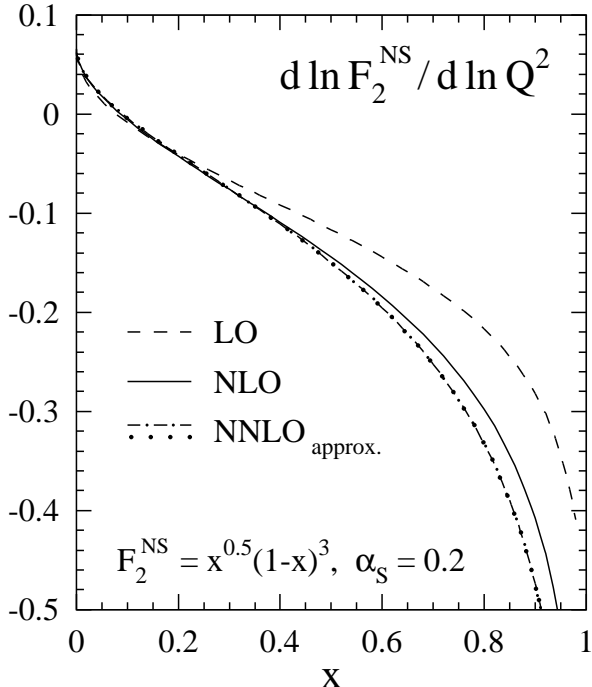


Figure 18. Convergence of F_2^{NS} slope ($\mu = Q, n_f = 4$).

actually dominated by the known NNLO coefficient functions, and is not so sensitive to the effect

of the only partially known NNLO anomalous dimensions. A slight decrease w.r.t. the NLO value of $\alpha_s(M_Z)$ was found for the NNLO $\alpha_s(M_Z)$.

9. CROSS-SECTIONS AT LOW Q^2

The transition region from DIS to photoproduction was earlier explored by the HERA experiments, reaching Q^2 values down to 0.11 GeV^2 [59]. These results were obtained by the ZEUS collaboration, after the installation in 1995 of a Beam-Pipe Calorimeter (BPC), increasing the acceptance for detecting the scattered electron at low angles. For the 1997 running, this device was supplemented by a Beam-Pipe Tracker (BPT). Allowing for a better background suppression as well as for an increased geometrical acceptance, the former measurement could be extended towards higher y and hence, down to $Q^2 = 0.045 \text{ GeV}^2$ and $x = 6 \cdot 10^{-7}$ [60]. Using an improved trigger setting and a suitable kinematic reconstruction method, increased the measurable region towards higher x values.

Figure 19 shows the reduced cross-section σ^{γ^*p} as function of Q^2 for fixed values of W , the total mass of the hadronic final state. The new measurement pins clearly down the transition from the rise of the cross-section with decreasing Q^2 to an asymptotic behaviour in the photoproduction limit. This “turnover” is very well described by the DL98 parametrisation (see section 10), whereas at high W values, the ALLM parametrisation is below the measured points. The total γp cross-section measurements from H1 and ZEUS tend to be lower than the expected values from an extrapolation of the low Q^2 DIS measurements.

10. PROTON MODELS AT LOW Q^2

Two presentations had models for the parton structure of hadrons at low scales in mind. One [61] argued on physical grounds for Gaussian parton momentum distributions with a width of a few hundred MeV related to the hadron size, for the valence quarks and the gluon, in the proton at rest. At low Q^2 scale (about 0.7 GeV^2) the thus-obtained parton distribution functions, including the gluon, are valence like. The model paramete-

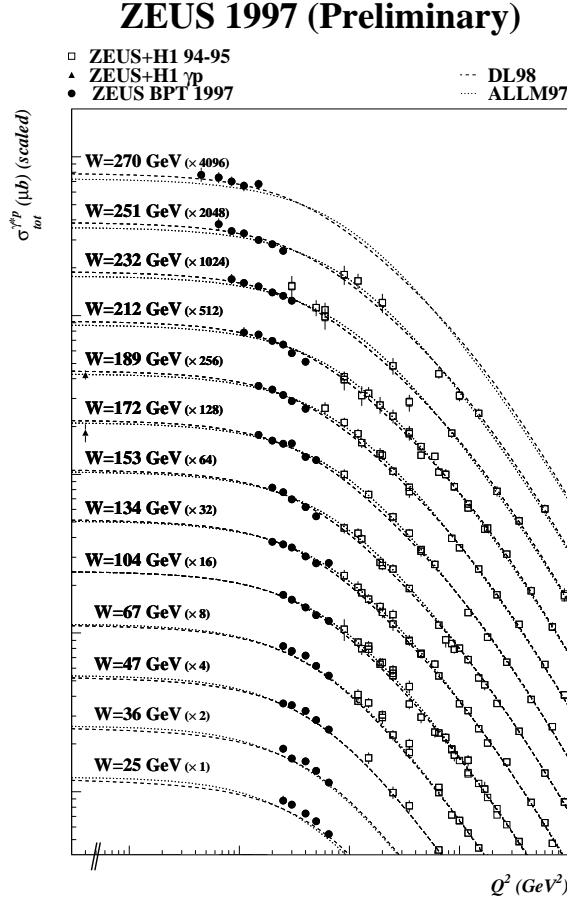


Figure 19. Reduced cross-section $\sigma^{\gamma^* p}$ as function of Q^2 for fixed values of W .

ters (essentially the widths of the Gaussians) in the distributions, when evolved to higher Q^2 , are fixed by fitting to the DIS data. The resulting structure function is too low at small x , and indicates a need for sea quark contributions. These are, as earlier, incorporated into the model via a pion cloud Ansatz. The distributions of the pions in the proton are similarly argued to be Gaussian, with a smaller width, and a free normalization. The final model, with 6 parameters, fits the data rather well with a χ^2 of 2 per degree of freedom.

In the second [62], the proton is surmised to consist at all scales of three (dressed) con-

stituent quarks. Deep-inelastic scattering probes of the proton at low Q^2 find these valence quarks, whereas at high Q^2 one probes their internal structure. The parton distributions in a proton are then generated from the constituent quark distributions by DGLAP-like evolution equations. This model has in the past been applied to e.g. leading particle production, as the constituent quarks, being the universal interface between hadronic and partonic quanta, are present in both the initial and final state of a scattering process. A simple Ansatz for the shape of the various densities was fixed by a fit to F_2 data at 12 GeV². The resulting model [62] agrees reasonably well with the rest of the HERA data.

Various other models focused in particular on the lower x structure function data. Haidt [63] showed that the $F_2(x, Q^2)$ data for $x < 0.001$ and $0.11 < Q^2 < 35 \text{ GeV}^2$, are very well described by the simple double logarithmic expression (motivated by the dominant boson-gluon fusion term in the partonic subprocesses [63])

$$F_2(x, Q^2) = 0.41\xi, \quad (8)$$

$$\xi = \log\left(\frac{0.04}{x}\right) \log\left(1 + \frac{Q^2}{0.5}\right),$$

i.e. the structure function, for the kinematic range mentioned, seems to depend only on ξ .

A Regge theory Ansatz for the structure function was proposed by Landshoff [64]

$$F_2(x, Q^2) = \sum_{i=1}^3 f_i(Q^2) x^{-\epsilon_i}, \quad (9)$$

with the ϵ_i representing the contributions from the Regge poles in the t -channel, and with a priori undetermined $f_i(Q^2)$. From older fits the values $\epsilon_1 = 0.08$ and $\epsilon_2 = -0.45$ (“soft pomeron” and f, a poles respectively) were used, together with $\epsilon_0 = 0.4$ (“hard pomeron”). For the Q^2 dependent coefficient functions a convenient parametrization involving 8 parameters was chosen. These were fixed in a very good quality fit to the $F_2(x, Q^2)$ data for $x < 0.07$ and $0 < Q^2 < 2000 \text{ GeV}^2$. A notable feature is the decrease of f_1 as Q^2 goes beyond 10 GeV². This was interpreted [64] as the soft pomeron contribution being of higher twist. A question mark

arises due the presence of a pQCD Regge pole at $\epsilon = 0$, close to 0.08, at any finite order in perturbation theory. However, it was argued [64] that resummed perturbation theory does not exhibit this pole.

In classical Generalized Vector Dominance (GVD) models, the photoproduction limit of the electroproduction cross section σ_{γ^*p} is expressed in those for $V + p$ scattering, where $V = \rho^0, \omega, \phi, J/\psi, \dots$, see [65, 66]. A generalization of GVD to electroproduction cross sections of exclusive vector meson production was presented [65]. Key to this extension is the inclusion of (destructively interfering) amplitudes for the diffractive transition $V'p \rightarrow Vp$, with V' a “excited state” of V . The model then expresses the exclusive vector meson electroproduction transverse and longitudinal (referring to the polarization of the γ^*) cross section in terms of the corresponding photoproduction cross section $\sigma_{\gamma p \rightarrow Vp}$, the effective transverse and longitudinal vector meson masses $M_{V,T/L}$, and a parameter ξ_V whose departure from the value 1 indicates vector meson-helicity dependence of the high-energy meson-nucleon cross section. The model was fitted to ρ^0, ϕ and J/ψ production data with 4 parameters ($M_{V,T/L}, \xi_V, \sigma_{\gamma p \rightarrow Vp}$). For the ρ^0 and ϕ cases, a good fit was obtained for $\xi_\rho(\xi_\phi) = 1.06(0.90)$, $M_{\rho,T}^2/M_\rho^2(M_{\phi,T}^2/M_\phi^2) = 0.68(0.43)$ and $M_{\rho,L}^2/M_\rho^2(M_{\phi,L}^2/M_\phi^2) = 0.71(0.60)$, and sensible values for the photoproduction cross sections. These fit results are in line with theoretical expectations [65].

11. BFKL

Leading logarithmic (LL) BFKL theory [67] for QCD scattering amplitudes at large s and medium $|t|$ (the Regge limit) enables one to resum all corrections of the form $\alpha_s^n \ln^n(s/|t|)$ for these amplitudes. In such scatterings gluon exchange dominates, and moreover, the gluon reggeizes, i.e. when including LL corrections in gluon quantum number exchange, the gluon propagator changes from $g^{\mu\nu}/k^2$ to $g^{\mu\nu}/k^2(s/|t|)^{\epsilon_g(k^2)}$, with $\epsilon_g(k^2)$ computed in perturbation theory, starting at $O(\alpha_s)$. If BFKL theory is applied to cross sections, the only object required, due to the

optical theorem, is the (imaginary part of the) color-singlet $t = 0$ exchange amplitude, which can be expressed in the four-point reggeized-gluon Green’s function at $t = 0$ and with color-singlet quantum numbers. In double-inverse Mellin form the BFKL equation [67] for this $t = 0$ Green’s functions reads

$$G(s, \mathbf{k}_1^2, \mathbf{k}_2^2) = \int \frac{d\gamma}{2\pi i} \frac{d\omega}{2\pi i} \left(\frac{s}{s_0} \right)^\omega \times \frac{1}{\omega - \bar{\alpha}_s \chi(\gamma)} \left(\frac{\mathbf{k}_1^2}{\mathbf{k}_2^2} \right)^\gamma, \quad (10)$$

where $\mathbf{k}_1^2, \mathbf{k}_2^2$ are the transverse momenta squared at both ends of the Green’s function, and $\bar{\alpha}_s = \alpha_s N_c / \pi$. One observes directly in this notation that the variable ω controls the large s behavior, while γ acts as an anomalous dimension. Performing the ω integral for the color-singlet $t = 0$ case by Cauchy’s theorem and the γ integral by saddle point ($\gamma_s^{LL} = 1/2$), the LL $s \rightarrow \infty$ behavior is $s^{\omega(\gamma_s)}$, corresponding to the BFKL pomeron ω -pole in (10).

The NLL [68] equation has the same form as (10), except that the χ function has a NLO part: $\bar{\alpha}_s \chi(\gamma) \rightarrow \bar{\alpha}_s(\mu^2)(\chi_0(\gamma) + \alpha_s(\mu^2)\chi_1(\gamma))$. Rather unsettling results of investigations into the changes due the next-to-leading logarithmic (NLL) BFKL equation on long-known leading logarithmic quantities were reported already at DIS’98. The effect on the LL pomeron intercept $\omega_0(\gamma_s^{LL})$ was shown to be rather dramatic

$$\begin{aligned} LL : \omega_0(\gamma_s^{LL}) &\simeq \bar{\alpha}_s 4 \ln 2, \\ NLL : \omega(\gamma_s^{LL}) &\simeq \omega_0(1 - 6.6\bar{\alpha}_s), \end{aligned} \quad (11)$$

i.e. except for very small α_s , the NLL intercept has a different sign. The present workshop featured a number of presentations that were devoted to understanding and improving this severely non-convergent behavior.

An approach aiming to restore the perturbative predictability of NLL BFKL theory, particularly relevant for deep-inelastic scattering with $\mathbf{k}_2^2 \simeq Q_0^2$, a low scale, and $\mathbf{k}_1^2 \gg Q_0^2$ was presented by Thorne [69]. The transverse momenta internal to the Green’s function connecting the hadron with the photon probe are well-known to diffuse into the infrared regime, the more so the smaller

x_B is. Thorne notes that both for the LL and NLL BFKL equations the Green's function may be factorized into a well-defined k_1^2 dependent factor $g(k_1^2, \omega)$ that includes the contribution from the diffusion into the UV, and a factor depending on the low scale Q_0 that includes the renormalon contributions due to diffusion into the infrared. Absorbing the latter function into the anyhow uncalculable initial condition, one may derive an effective anomalous dimension $\Gamma(\omega, \alpha_s(k^2))$ governing the gluon evolution from $\partial \ln g(k^2, \omega) / \partial k^2$. Using BLM [70] scale fixing, this anomalous dimension may be expressed in terms of the LO gluon splitting function, but with $\alpha_s(k^2)$ replaced by $\alpha_s^{eff}(\tilde{k}^2(x_B))$ which is smaller than $\alpha_s(k^2)$ due to the inclusion of the effects of diffusion into the UV. (The BLM approach to improving the perturbative behavior of the BFKL intercept (11) was also discussed by Lipatov [71].) Translating this scale setting procedure for the physical anomalous dimension (6) leads even at LO to a better fit to DIS data than the MRST standard NLO fit [69].

A somewhat different approach was discussed by Ciafaloni [72]. In contrast to the LL BFKL equation, the NLL version is sensitive to the choice of the reference scale s_0 in (10). If $\mathbf{k}_1^2 \gg \mathbf{k}_2^2$, one would choose $s_0 = \mathbf{k}_1^2$, so that the Green's function behaves as $[\bar{\alpha}_s \ln(s/\mathbf{k}_1^2) \ln(\mathbf{k}_1^2/\mathbf{k}_2^2)]^n$, but if one chooses $s_0 = \sqrt{\mathbf{k}_1^2 \mathbf{k}_2^2}$ the double-log series differs from the previous one by, again, large double logarithms. To render the Green's function insensitive to the choice of s_0 , one must resum these double logarithms. The symmetric way (i.e. including the case $\mathbf{k}_2^2 \gg \mathbf{k}_1^2$) of doing this is to resum the $1/\gamma$ and $1/(1-\gamma)$ terms in $\chi(\gamma)$ to all orders, which leads effectively to a shift of γ by $\omega/2$, and an improved kernel $\chi(\gamma, \omega)$, now depending on ω . This resummation also restabilizes the γ integral in (10), which the NLL effects had destabilized. Furthermore, renormalization group arguments for $\mathbf{k}_1^2 \gg \mathbf{k}_2^2 = \mathbf{k}_0^2$, lead to a factorized form of the Green's function, one factor being sensitive to \mathbf{k}_0^2 only, and hence non-perturbative, the other only dependent on \mathbf{k}_1^2 , presumably much more amenable to perturbative treatment. Using the improved kernel function

$\chi(\gamma, \omega)$ for this latter factor, an effective anomalous dimension $\gamma(\omega, t)$ ($t \sim \ln(\mathbf{k}_1^2)$) may again be derived, which is very similar to the DGLAP value until it diverges for a critical $\omega_c(t) \simeq 0.2$ much lower than the saddle-point value $\omega_s(t)$, which is $\simeq 0.5$ in LL (11). Moreover, the thus-generalized NLL BFKL is free of instabilities.

Del Duca [73] discussed the application of LL and NLL BFKL theory to dijet production at large rapidity intervals [74], and reviewed the ingredients entering the NLO calculation of the BFKL kernel, such as the NNLO reggeization of the gluon, and the real and virtual corrections to the Lipatov vertex. Some of these ingredients are equally necessary for exact finite order QCD calculations [75], and in this sense BFKL theory inspires progress beyond its own domain. NLL BFKL allows, in contrast to the LL case, momentum conservation, running coupling effects, and jet substructure. It was also pointed out, as in some of the other presentations, that a not-yet-completed part of full NLL BFKL theory is the NLO calculation of the impact factors, the effective vertices which the four point reggeized-gluon Green's function connects (see [76] for a pictorial representation). A way to control the size of the NLL correction with a cut on the rapidities of the gluons emitted along the ladder [77] was also mentioned.

Fadin [76] pointed out that the key ingredient to the BFKL approach is the reggeization of the gluon and quark in the Regge limit, a phenomenon that, although shown to hold in LL, and in NLL through $O(\alpha_s^2)$, requires further tests. The factorization of a scattering amplitude in the Regge limit in terms of impact factors and a t -channel Green's function provides the possibility to conduct such a test by considering not just color-singlet $t = 0$ exchange, but other color channels, and $t \neq 0$. Self-consistency of this factorized approach leads to non-trivial, quite restrictive "bootstrap" conditions, such as the requirement that two interacting reggeized gluons exchanged with gluon quantum numbers correspond again to a reggeized gluon. The validity of some of these bootstrap conditions has been verified, while others are under investigation [76].

The dynamics of reggeized gluons together with

elementary ones can be summarized in an effective action for these degrees of freedom [71]. From this action a Hamiltonian can be derived that depends only on the transverse coordinates (which may be represented as complex numbers) of the reggeized gluons. At LL this Hamiltonian can be exactly (at NLL approximately) factorized holomorphically in these coordinates, allowing the application of the powerful tools of two-dimensional conformal field theory and exactly solvable models to analyze the wave functions of compound reggeized gluon-states in the t -channel. Using such tools, Lipatov [71] showed that the intercept ω^{Odd} corresponding three-reggeon compound state, the charge conjugation-odd Odderon, is identical to the intercept (11) of the pomeron, a compound state of two such reggeized gluons.

12. UNITARIZATION AND LATTICE RESULTS

When the DIS data are plotted as $\partial F_2(x, Q^2)/\partial \ln Q$ vs. x , where to each value of x a value of Q^2 is assigned (viz. the average Q in the x bin considered), the partial derivative rises with decreasing x until about 0.001 (which is correlated with $\langle Q^2 \rangle \simeq 5 \text{ GeV}^2$), then falls again as x is lowered further. The turnover is roughly in the kinematic region where the transition from perturbative to non-perturbative dynamics is expected to take place. This plot was shown by Yoshida [11] for the ZEUS data. The lowest experimental point has an x -value of a few times 10^{-6} , corresponding with an average Q^2 of about 0.1 GeV^2 . A good approximation at small x in terms of the gluon density is given by [11]

$$\partial F_2^{SC}(x, Q)/\partial \ln Q \simeq \text{const } xg(2x, Q^2). \quad (12)$$

This plot and its interpretation were discussed in the context of small x screening effects by Gotsman [78]. A leading twist DGLAP description of this curve has trouble following the decrease as x descends below 0.001. Taking screening corrections to QCD evolution in account via an eikonal approach, the slope was expressed as

$$\frac{\partial F_2^{SC}(x, Q)}{\partial \ln Q} = \frac{\partial F_2^{DGLAP}(x, Q)}{\partial \ln Q} D(x, Q^2), \quad (13)$$

where $D(x, Q^2)$ is an explicitly calculated correction factor that accounts for the screening corrections. Substituting the experimental correlation $\langle Q^2 \rangle(x)$ [11] produces a curve for $\partial F_2(x, Q^2)/\partial \ln Q$ vs. x that agrees well with the data.

Another, more algebraic but also physical understanding for the mechanism of unitarization of the large s , fixed t cross section was presented by Lam [79]. In this kinematic limit the powerlike growth $s^{\alpha(t)}$ of the total cross section implied by the leading log BFKL equation, violates, in principle, the Froissart unitarity bound $\ln^2(s)$. It was shown [79] that many-gluon exchange between two fast moving particles may be seen as the interaction of color-octet quasi-particles emitted in a coherent state. The full leading log exchange amplitude factorizes in the s -channel into contributions from sets of $1, 2, \dots$ exchanged quasi-particles, each set corresponding to a Reggeon. At fixed impact parameter b it is then given by the unitary expression

$$A(s, b) = 1 - \exp \left(2i \sum_m \delta_m(s, b) \right), \quad (14)$$

where the sum is over the contributions δ_m of the sets.

A status report on an effort to compute power corrections to structure functions numerically on the lattice was given by Schierholz [80]. When one contemplates computing (moments of) a structure function on the lattice, and extracts twist-4 power corrections from this, via

$$F(N, Q^2) = C_2(N, \frac{Q^2}{\mu^2}) \langle H | O_2^N(\mu^2) | H \rangle \quad (15) \\ + \frac{C_4(N, Q^2/\mu^2)}{Q^2} \langle H | O_4^N(\mu^2) | H \rangle + \dots$$

one is immediately confronted with definition ambiguities of the two terms on the right hand side, due to renormalon effects. To avoid this, and automatically take care of mixing complications, both the Wilson coefficients C_2, C_4 and the operator matrix elements were computed on the lattice. As a byproduct one may thereby verify the OPE, whose first two terms are listed in (15). First results for F_2 , in the quenched approximation,

indicate a -25% correction at $Q^2 = 5 \text{ GeV}^2$ due to twist 4 contributions. The few leading twist moments of F_2 computed in this way on the lattice agree with an analytic calculation using the MRST densities.

13. HIGH Q^2 AND SEARCHES

Since 1998, HERA is producing e^-p collisions, with an increased proton beam energy of 920 GeV, leading to a center of mass energy of 320 GeV. Figure 20 compares the single differential cross-sections $d\sigma/dQ^2$ for neutral and charged

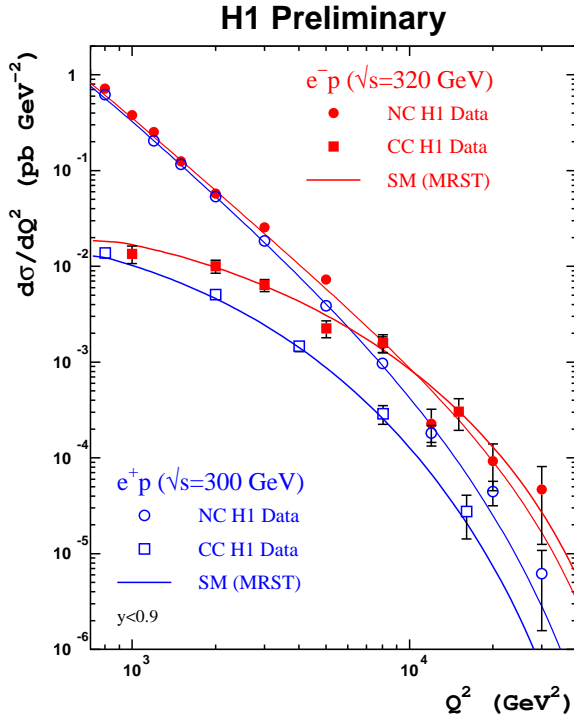


Figure 20. $d\sigma/dQ^2$ for neutral and charged currents in e^+p and e^-p from H1. Similar measurements were presented by the ZEUS collaboration.

current interactions at high Q^2 to the e^+p measurements from the data taken in 1994 – 1997 at $\sqrt{s} = 300 \text{ GeV}$ [33, 34]. In Neutral Currents, at $Q^2 < 1000 \text{ GeV}^2$, where electroweak effects are

small, almost no difference is visible in the cross-section, except an small increase in the e^+p due to the higher center of mass energy. At higher Q^2 however, the contribution to the cross-section from $\gamma - Z$ interference is destructive in the case of e^+ scattering and constructive for e^- scattering. No significant deviation from the expected cross-section is seen in the new measurement.

In charged current interactions, mainly the d -quarks are probed in e^+ running, whereas the rise in the cross-section for the e^- running is due to the probe of the u -densities. At high Q^2 , the difference in the cross-section is nearly one order of magnitude, as $\sigma(e^+p) \propto (1-y)^2(d+s)$ and $\sigma(e^-p) \propto (u+c)$. From the Q^2 dependence of the CC cross-section the spacelike propagator mass M_W can be determined, when fixing the well measured G_F value. The obtained values from the e^+ running are

$$\begin{aligned} \text{H1 :} & \quad 81.2 \pm 3.3(\text{stat}) \pm 4.3(\text{syst}) \text{ GeV} \\ \text{ZEUS :} & \quad 81.4^{+2.7}_{-2.6}(\text{stat})^{+2.0}_{-2.0}(\text{syst})^{+3.3}_{-3.0}(\text{PDF}) \text{ GeV} \end{aligned}$$

The figure 21 shows the single differential cross-section compared to different values of M_W . The M_W measurement from ZEUS [33] without fixing G_F is consistent with the previous result, although

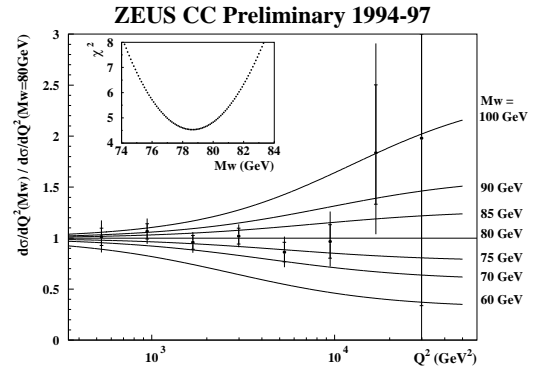


Figure 21. $d\sigma/dQ^2$ compared to NLO-QCD fit with various values of M_W from the ZEUS experiment. A similar measurement was presented by H1.

the errors are bigger (except for the PDF dependence). A consistency check using the Standard Model relation between G_F, M_W, M_Z and M_H is in good agreement with the world average on M_W .

The signature for real W production at HERA are events with isolated leptons and missing p_T . During the 1994-1997 running, 1 event with an isolated e^+ and 5 events with isolated μ were found by the H1 collaboration [81], whereas ZEUS [82] found three events with isolated e^+ and no μ events. Figure 22 shows the kinematic properties of these events compared to Monte

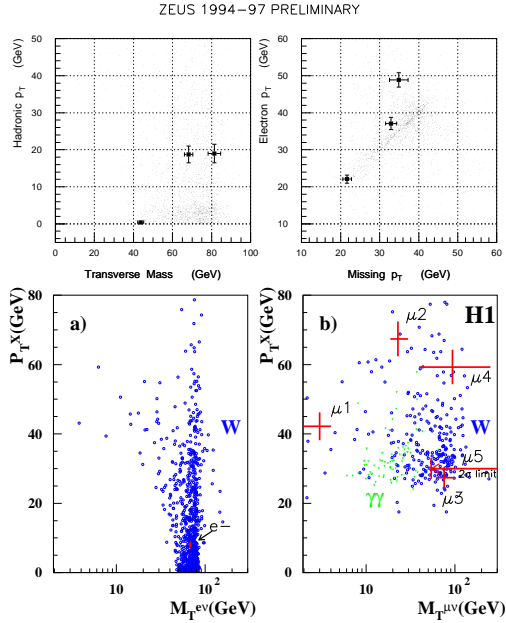


Figure 22. Kinematic properties of events with and isolated lepton compared to W production MC seen in the ZEUS (upper plots) and the H1 (lower plots) experiments.

Carlo Simulation of W production. The e^+ events of H1 and ZEUS are both compatible with W production and the expected background from NC events. The 3 H1 muon events however, lie in kinematic regions, where W production is unlikely. During the 1998 running, one e^- event

has been found by ZEUS and none by H1, again compatible with the expectation, and none of the outstanding μ events.

From the single differential cross-section limits on Contact Interactions can be determined [83, 84], which are the most general way to search at low energy effects of possible physics beyond the Standard Model at much higher scales, in particular on vector $eeqq$ contact interaction, where only weak limits exist, compared to scalar or tensor terms. From a global analysis including HERA, LEP and Tevatron data any contact interaction below 2.1 TeV can be excluded [84]. Detailed limits on particular channels can be found in [81, 82]. Constraints from the existing data can be used, in order to evaluate the possibility of discovery in future running periods. Figure 23 [84] is showing 95% C.L. of a global model,

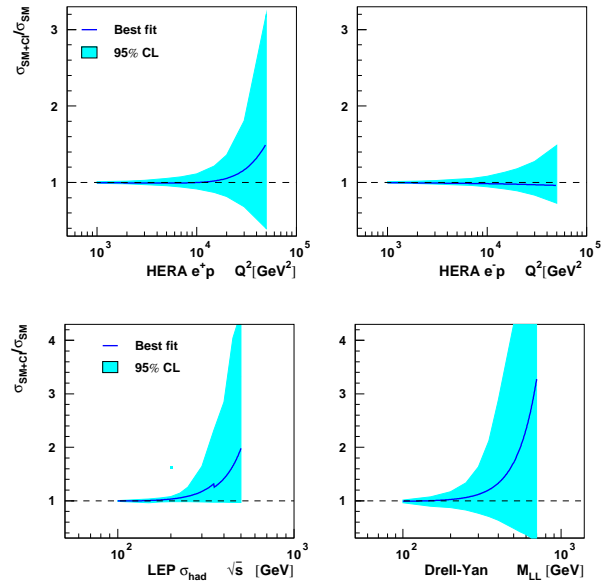


Figure 23. 95% CL limit band on the ratio of predicted SM cross-section for e^+p and e^-p NC DIS at HERA, total hadronic cross-section at LEP/NLC and Drell-Yan production at the Tevatron.

assuming Contact Interactions to couple only e to u and d . The constraints on e^+p are shown to be much weaker, than for e^-p . For hadronic production in e^+e^- interactions significant deviations from the cross-section will be only possible at the NLC, with $\sqrt{s} > 300$ GeV, in contrast to deviations in the Drell-Yan cross-section, where large deviations are still allowed at the Tevatron energies.

Acknowledgments

We would like to thank all speakers for their talks and contributions, and the organizers for their efforts and excellent support. Special thanks to our scientific secretaries, D. Eckstein and R. Wallny.

REFERENCES

1. M. Glück, E. Reya and A. Vogt, Eur. Phys. J. **C5**, 461 (1998) hep-ph/9806404.
2. A.D. Martin, R.G. Roberts, W.J. Stirling and R.S. Thorne, Eur. Phys. J. **C4**, 463 (1998) hep-ph/9803445.
3. H.L. Lai *et al.*, CTEQ Collab., hep-ph/9903282.
4. S. Kuhlmann, these proceedings.
5. R.S. Thorne and R.G. Roberts, Phys. Lett. **B421** (1998) 303, *ibid.* Phys. Rev. **D57** (1998) 6871.
6. M.A.G. Aivazis, J.C. Collins, F.I. Olness and W.K. Tung, Phys. Rev. **D50** (1994) 3102; J.C. Collins, Phys. Rev. **D58** (1998) 094002.
7. A.D. Martin *et al.*, hep-ph/9906231.
8. U.K. Yang and A. Bodek, Phys. Rev. Lett. **82** (1999) 2467.
9. M. Botje, hep-ph/9905518.
10. F. Zomer, these proceedings.
11. R. Yoshida, ZEUS Collab., these proceedings; ZEUS Collab., J.Breitweg *et al.*, Euro. Phys. J. **C7** (1999) 609.
12. J. Zacek, H1 Collab., these proceedings.
13. H1 Collab., S. Aid *et al.*, Nucl. Phys. **B470** (1996) 3; ZEUS Collab., M. Derrick *et al.*, Z. Phys. **C72** (1996) 399.
14. V. Arkadov, H1 Collab., these proceedings.
15. H1 Collab., C. Adloff *et al.*, Phys. Lett. **393B** (1997) 452.
16. U.-K. Yang, CCFR Collab., these proceedings.
17. CCFR Collab., M. Vakili *et al.*, hep-ex/9905052 *submitted to Phys. Rev. Lett.*; CCFR Collab., W.E. Seligman *et al.*, Phys. Rev. Lett. **79** (1997) 1213.
18. CDHSW Collab., J.P. Berge *et al.*, Z. Phys. **C 49** (1991) 187.
19. CHORUS Collab., P. Annis *et al.*, Phys.Lett. **B435** (1998) 458.
20. R. Oldeman, CHORUS Collab., these proceedings.
21. A. Sidorov *et al.*, IHEP-JINR Collab., hep-ex/9905038.
22. NMC Collab., M. Arneodo *et al.*, Phys. Rev. **D50** (1994) 1.
23. A. Miller, HERMES Collab., these proceedings; HERMES Collab., K. Ackerstaff *et al.*, Phys. Rev. Lett. **81** (1998) 5519.
24. D. Isenhower, E866 Collab., these proceedings; E866/NuSea Collab., E.A. Hawker *et al.*, Phys. Rev. Lett. **80** (1998) 3715.
25. A. Szczurek *et al.*, hep-ph/9905516; N.N. Nikolaev, W. Schafer, A. Szczurek and J. Speth, Phys. Rev. **D60** (1999) 014004 hep-ph/9812266.
26. A. Bodek, CDF Collab., these proceedings.
27. CDF Collab., F. Abe *et al.*, Phys.Rev. **D59** (1999) 052002.
28. W.T. Giele, E.W. Glover and D.A. Kosower, Nucl. Phys. **B403** (1993) 633 hep-ph/9302225.
29. C. Balazs and C.P. Yuan, Phys. Rev. **D56** (1997) 5558 hep-ph/9704258.
30. CDF Collab., F. Abe *et al.*, Phys.Rev.Lett. **81** (1998) 5754.
31. L. Frankfurt and M. Strikman, Phys. Rep. **160** (1998) 235.
32. A. W. Thomas, W. Melnitchouk, hep-ph/9708484.
33. R. Pawlak, ZEUS Collab., these proceedings.
34. B. Reisert, H1 Collab., these proceedings.
35. ZEUS Collab., J.Breitweg *et al.*, DESY 99-056 (1999) *subm. to Euro. Phys. J.*

36. H1 Collab., C. Adloff et al., Z. Phys **C74** (1997) 191;
ZEUS Collab., J. Breitweg et al., Z. Phys. **C74** (1997) 207.
37. C. Keppel, E97-010 Collab., these proceedings.
38. A. Akopian, CDF Collab., these proceedings.
39. CDF. Collab., F. Abe et al., Phys. Rev. Lett. **77** (1996) 438.
40. V.D. Elvira, DØ Collab., hep-ex/9906020.
41. DØ Collab., B. Abott et al., Phys. Rev. Lett. **82** (1999) 2451.
42. F.S. Chlebana, CDF Collab., these proceedings.
43. H. Schellman, DØ Collab., FERMILAB-Conf-99/170-E.
44. M. Begel, E706 Collab., these proceedings.
45. E706 Collab., L. Apanasevich et al., Phys. Rev. Lett. **81** (1998) 2642.
46. P. Aurenche, A. Douiri, R. Baier, M. Fontannaz and D. Schiff, Phys. Lett. **140B** (1984) 87.
47. S. Kuhlmann, CDF Collab., these proceedings.
48. C. Adloff, H1 Collab., these proceedings.
49. I. Redondo, ZEUS Collab., these proceedings.
50. H1 Collab., C. Adloff et al., Z. Phys. **C72** (1996) 563;
ZEUS Collab., J. Breitweg et al., Phys. Lett. **B407** (1997) 402.
51. E. Laenen, S. Riemersma, J. Smith and W.L. van Neerven, Nucl. Phys. **B392** (1993) 162, 229;
S. Riemersma, J. Smith and W.L. van Neerven, Phys. Lett. **B347** (1995) 43;
B.W. Harris and J. Smith, Nucl. Phys. **B452** (1995) 109; Phys. Rev. **D57** (1998) 2806.
52. J. Smith, these proceedings.
53. M. Buza, Y. Mاتيounine, J. Smith, W.L. van Neerven, Eur. Phys. J. **C1** (1998) 301; Phys. Lett. **B411** (1997) 211.
54. W. Bernreuther and W. Wetzel, Nucl. Phys. **B197** (1982) 228;
W. Bernreuther, *Annals of Physics* **151** (1983) 127;
S.A. Larin, T. van Ritbergen and J.A.M. Vermaseren, Nucl. Phys. **B438** (1995) 278;
K.G. Chetyrkin, B.A. Kniehl and M. Steinhauser, Phys. Rev. Lett. **79** (1997) 2184 hep-ph/9706430.
55. J. Blümlein, these proceedings;
J. Blumlein and S. Kurth, hep-ph/9810241.
56. V. Ravindran et al, hep-ph/9905513;
J. Blumlein, V. Ravindran and W.L. van Neerven, Acta Phys. Polon. **B29** (1998) 2581 hep-ph/9806355.
57. A. Kataev et al, hep-ph/9904332;
A.L. Kataev, G. Parente and A.V. Sidorov, hep-ph/9905310.
58. A. Vogt, hep-ph/9906337.
59. H1 Collab., C. Adloff et al., Nucl.Phys. **B497** (1997) 3;
ZEUS Collab., M. Derrick et al., Z. Phys. **C69** (1996) 607;
ZEUS Collab., J. Breitweg et al., Phys. Lett. **B407** (1997) 432.
60. C. Amelung, ZEUS-Collab., hep-ex/9905055.
61. A. Edin et al., these proceedings;
A. Edin and G. Ingelman, Phys. Lett. **B432** (1998) 402, hep-ph/9803496.
62. A.N. Khorramian et al., these proceedings;
F. Arash and A.N. Khorramian, hep-ph/9904264.
63. D. Haidt, these proceedings.
64. P. Landshoff, hep-ph/9905230;
J.R. Cudell, A. Donnachie and P.V. Landshoff, Phys. Lett. **B448** (1999) 281, hep-ph/9901222.
65. D. Schildknecht, hep-ph/9906216;
D. Schildknecht, G.A. Schuler and B. Surrow, Phys. Lett. **B449** (1999) 328 hep-ph/9810370.
66. W. van Neerven, these proceedings.
67. L.N. Lipatov, Sov. J. Nucl. Phys. 23 (1976) 338; Ya. Balitskii and L.N. Lipatov, Sov. J. Nucl. Phys. 28 (1978) 822;
E.A. Kuraev, L.N. Lipatov, and V.S. Fadin, Sov. Phys. JETP 44 (1976) 443; *ibid.* 45 (1977) 199.
68. V.S. Fadin and L.N. Lipatov, Phys. Lett. **B429** (1998) 127;
G. Camica and M. Ciafaloni, Phys. Lett. **B430** (1998) 349.
69. R.S. Thorne, hep-ph/9906323;
R.S. Thorne, hep-ph/9901331.
70. S.J. Brodsky, G.P. Lepage and P.B. Macken-

- zie, Phys. Rev. **D28** (1983) 228.
71. L. Lipatov, these proceedings. S.J. Brodsky, V.S. Fadin, V.T. Kim, L.N. Lipatov and G.B. Pivovarov, hep-ph/9901229.
 72. M. Ciafaloni, hep-ph/9905534; M. Ciafaloni and D. Colferai, Phys. Lett. **B452** (1999) 372 hep-ph/9812366; M. Ciafaloni, D. Colferai and G.P. Salam, hep-ph/9905566.
 73. V. Del Duca, hep-ph/9906278.
 74. V. Del Duca and C.R. Schmidt, Phys. Rev. **D57** (1998) 4069 hep-ph/9711309; V. Del Duca and C.R. Schmidt, Phys. Rev. **D49** (1994) 4510 hep-ph/9311290.
 75. Z. Bern, V. Del Duca, W.B. Kilgore and C.R. Schmidt, hep-ph/9903516;
 76. V. Fadin, these proceedings. V.S. Fadin, R. Fiore and A. Papa, hep-ph/9812456; V.S. Fadin and R. Fiore, Phys. Lett. **B440** (1998) 359 hep-ph/9807472.
 77. C. Schmidt, hep-ph/0091397.
 78. E. Gotsman, these proceedings. E. Gotsman, E. Levin, U. Maor and E. Naf-tali, Nucl. Phys. **B539** (1999) 535 hep-ph/9808257.
 79. C.S. Lam, hep-ph/9905522; R. Dib, J. Khoury, and C.S. Lam, hep-ph 9902429.
 80. G. Schierholz, hep-ph/9906320.
 81. H.-C. Schlutz-Coulon, H1 Collab, these pro-ceedings.
 82. R. Galea, ZEUS Collab., these proceedings.
 83. J. Scheins, H1 Collab., these proceedings.
 84. P. Zarnecki, ZEUS Collab., hep-ph/9905565.